Journal of Crystal Growth 106 (1990) 629–634
North-Holland

PHASE DIAGRAM OF $Zn_{2x}(CuIn)_yMn_{2z}Te_2$ ALLOYS

Rafael TOVAR and Miguel QUINTERO

Centro de Estudios de Semiconductores, Departamento de Física, Universidad de Los Andes, Mérida, Venezuela

and

Champa NEAL and John C. WOOLLEY

Ottawa–Carleton Institute for Physics, University of Ottawa, Ottawa, Ontario, Canada K1N 6N5

Received 12 January 1990; manuscript received in final form 1 June 1990

The T versus composition phase diagram of the alloy system $Zn_{2x}(CuIn)_yMn_{2z}Te_2$ was investigated in the range $0 < z < 0.80$ by differential thermal analysis and X-ray diffraction measurements. Samples were prepared for various lines of constant x/y ratio and the $T(z)$ data determined for each line. From the values of lattice parameter determined for all samples, the limits of single-phase solid solution were estimated. In addition to liquidus and solidus curves, the zinc-blende–chalcopyrite and Mn-disordered–Mn-ordered transition lines were determined, these phase fields being the ones of interest in the measurements of optical energy gap and of magnetic properties.

1. Introduction

Most of the work [1,2] on semimagnetic semiconductor alloys has been concerned with alloys of the form $II_{1-z}Mn_zVI$. However, similar alloys can be produced from the chalcopyrite I–III–VI_2 compounds, the ternary analogs of the II–VI compounds. The crystallography and optical energy gap values of a number of alloy systems of the form $(I–III)_{1-z}Mn_{2z}Te_2$ have been investigated [3–7], and also the work has been extended to the more general $Cd_{2x}(I–III)_yMn_{2z}Te_2$ $(x+y+z=1)$ alloys. The magnetic and ESR results for various $(I–III)_{1-z}Mn_{2z}Te_2$ alloys have been reported [8,9].

These chalcopyrite-based alloys are of interest because, depending upon the heat-treatment, the alloys can be produced with the Mn atoms either at random or ordered (or partially ordered) on the cation sublattice. The optical energy gap values and the magnetic behavior are very different in the two different conditions [7–10]. Before a detailed investigation of the effects of this ordering can be carried out, it is necessary to choose the heat-treatment of the alloys so as to produce the required ordered or disordered condition. For this purpose, a detailed knowledge of the T versus composition phase diagram is required. Most of the work so far has been concerned with the Cd-based alloys (e.g., refs. [3,4]), with little work on Zn-based materials. Garbato and Ledda [11] investigated the crystallography of the $Zn_{2x}(CuIn)_{1-x}Te_2$ alloys and recently the present authors have given the crystallography and optical energy gap values of the $Zn_{2x}(CuIn)_yMn_{2z}Te_2$ and $Zn_{2x}(AgIn)_yMn_{2z}Te_2$ alloys [12]. In the present work, this investigation of the Zn-based alloys has been extended to the study of the $T(z)$ diagrams of various sections of the alloy system $Zn_{2x}(CuIn)_yMn_{2z}Te_2$ $(x+y+z=1)$.

2. Preparation of samples and experimental measurements

All of the alloys used were produced by the usual melt and anneal technique [12,13]. The components of each 1.5 g sample were sealed under

vacuum in small quartz ampoules which had previously been carbonized to prevent interaction of the alloy with the quartz, melted together at 1150 °C and then annealed to equilibrium. As in all such multicomponent alloys, the appropriate temperature of anneal is not easily determined until the T versus composition phase diagram is known for each section. However the results for the sections $(CuIn)_{1-z}Mn_{2z}Te_2$ and $Zn_{2x}(CuIn)_{1-x}Te_2$ already investigated [6,1], show that an annealing temperature of 600 °C should be satisfactory, and this value was used here. Equilibrium at fairly low temperatures is needed if peaks corresponding to order–disorder and chalcopyrite–zinc-blende transitions are to be observed in the heating DTA runs. It has been found that at least 20–30 days of annealing is necessary to obtain equilibrium conditions at 600 °C, since long-range diffusion may be required after the initial cooling from the melt. However, once this has been achieved, the zinc-blende–chalcopyrite and order–disorder transitions, which occur below 600 °C in these systems but which involve only short-range diffusion, can occur in much shorter times. In order to produce useful $T(z)$ diagrams, samples were prepared for the sections given by $x = 3y$, $x = y$, $y = 3x$, $x = 0$ and $z = 0$ as shown in fig. 1. Since the interest of the programme is in semimagnetic semiconductors, values of z up to an upper limit of 0.8 only were used, and the Mn-rich phases were not investigated.

X-ray powder photographs, either Guinier or Debye–Scherrer, were used to check the conditions of the annealed samples and to determine the phases that were present. Values of lattice parameter were determined for the zinc-blende and chalcopyrite phases, these results having been reported previously [12].

Phase transition temperatures were obtained from DTA measurements [14], using a closed tube configuration and with silver or gold used as the reference material. The charge was a powdered alloy of approximately 100 mg weight. The temperatures of the sample and of the reference were measured with chromel–alumel thermocouples, the difference signal between sample and reference and also the temperature signal being simultaneously registered on a two-pen chart recorder. Each phase transition temperature was determined from the base-line intercept of the tangent to the

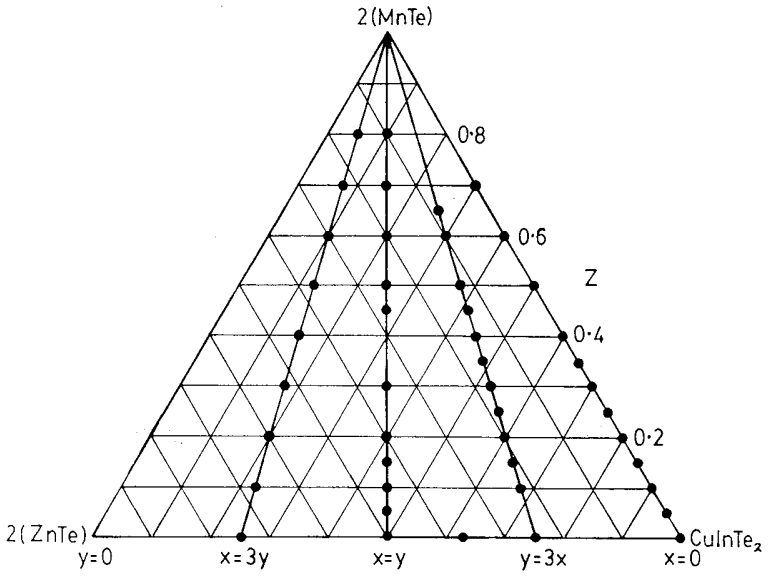

Fig. 1. Composition diagram for the $Zn_{2x}(CuIn)_yMn_{2z}Te_2$ alloys. (●) Composition of alloys used in the present work.

leading edge of the peak in the difference signal. Both heating and cooling runs were made for each sample.

3. Results and discussion

In previous work on the $Zn_{2x}(CuIn)_yMn_{2z}Te_2$ alloys [12], lattice parameter values for samples slowly cooled to room temperature were used to determine the composition ranges of the various single-phase fields involving the zinc-blende (β) and chalcopyrite (α) phases. With regard to the T versus composition data, the $T(x)$ diagram for the $Zn_{2x}(CuIn)_{1-x}Te_2$ section, i.e. $z = 0$, was given by Garbato and Ledda [11] and part of that diagram has been repeated here. The diagram of Garbato and Ledda indicates that an $(\alpha + \beta)$ two phase range occurs, extending at 400 °C from $x = 0.09$ to $x = 0.28$, which was not observed in the present work. However, the values of lattice parameter given [11] indicate that at each value of x in that range, the chalcopyrite and zinc-blende phases

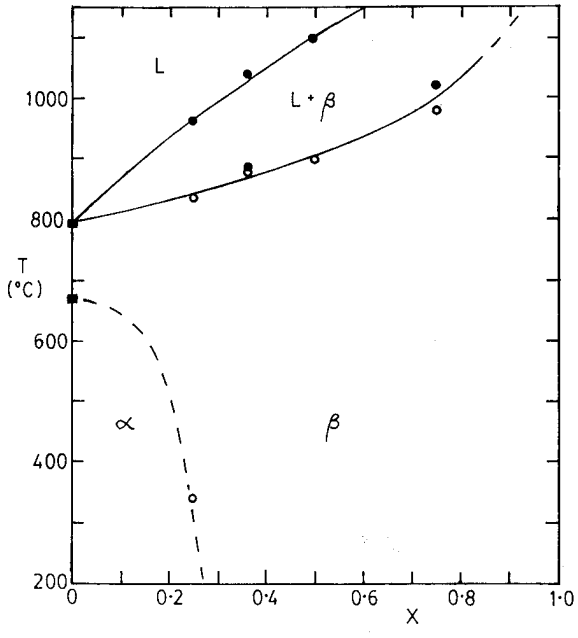

Fig. 2. $T(x)$ diagram for $Zn_{2x}(CuIn)_{1-x}Te_2$ section, (i.e. $z = 0$); α is the chalcopyrite and β the zinc-blende structure: (○) heating run; (●) cooling run; (■) from Garbado and Ledda [11].

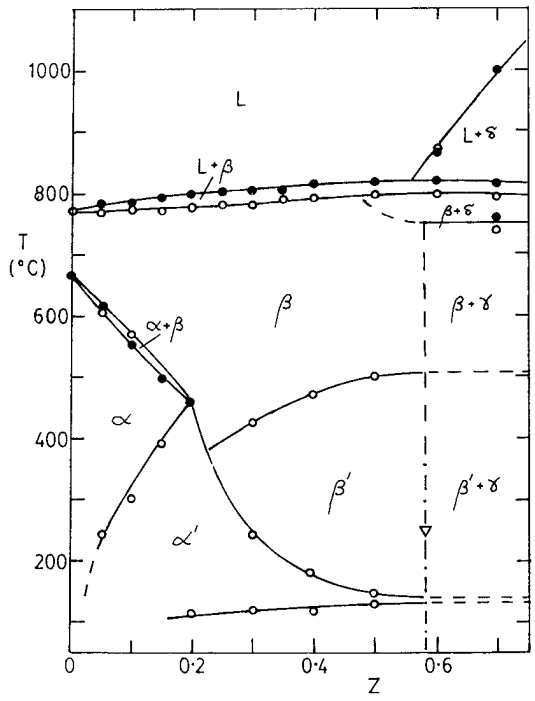

Fig. 3. $T(z)$ diagram for the $(CuIn)_{1-z}Mn_{2z}Te_2$ section (i.e. $x = 0$): α is the Mn-disordered chalcopyrite, α' the Mn-ordered chalcopyrite, β the Mn-disordered zinc-blende, β' the Mn-ordered zinc-blende, and γ and δ are the NiAs and NaCl structures of MnTe, respectively; (○) heating run; (●) cooling run; (▽) from X-ray data.

show the same value of a. As was pointed out in recent work on the lattice parameter values of the $Zn_{2x}(CuIn)_yMn_{2z}Te_2$ alloys [12], the various results indicate that the apparent two phase behaviour is due to an order–disorder reaction which is very slow because of the relatively low ordering temperature. Thus the apparent two phase field represents non-equilibrium conditions. In fig. 2, in the $T(x)$ diagram of this section the boundary between the α and β phases is shown as a single line. Recently the $T(z)$ diagram has been obtained for the $(CuIn)_{1-z}Mn_{2z}Te_2$ section [5], i.e. $x = 0$ and for comparison purposes this diagram is shown in fig. 3. For the case of the $Zn_{1-z}Mn_zTe$ section, i.e. $y = 0$, no data seem to be available.

The $T(z)$ diagrams for the section $y = 3x$, $x = y$ and $x = 3y$ are shown in figs. 4, 5, and 6 respectively. In these diagrams, boundaries determined directly from DTA measurements are shown as

solid lines. However, some boundaries cannot be determined from the DTA data and these need to be estimated from the lattice parameter and energy gap values determined previously [12]. These boundaries are shown as dash-dotted lines in the $T(z)$ diagrams, while dashed lines have been used to indicate lines which are estimates only. The range of the present experimental results is from room temperature to 1200 °C. Hence, since the melting point of ZnTe is 1290 °C [11], for the present alloys it was not possible to obtain values for the liquidus curves beyond $z = 0.5$.

As has been shown previously [15], $CuInTe_2$ has the chalcopyrite (α) structure up to 670 °C and then becomes zinc-blende (β) up to its melting point at 770 °C. Figs. 2, 3, and 4 show that in the section $z = 0$, $x = 0$, and $y = 3x$ both the α and β phases are present. For the $x = y$ and

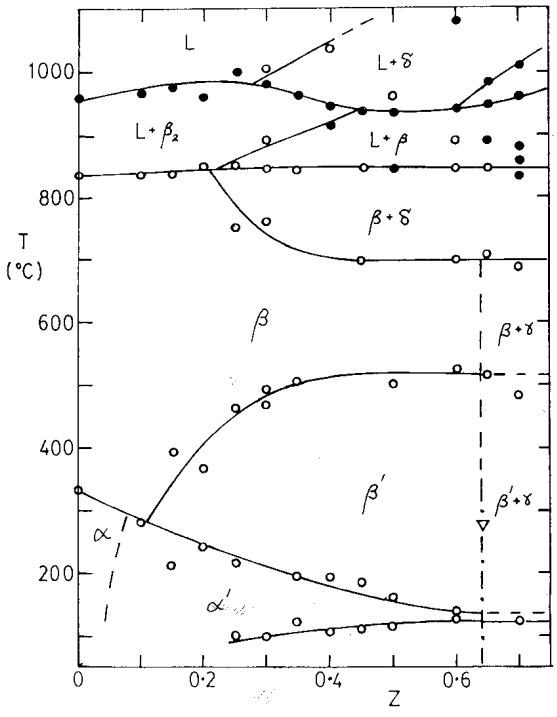

Fig. 4. $T(z)$ diagram for the $y = 3x$ section: α is the Mn-disordered chalcopyrite, α' the Mn-ordered chalcopyrite, β the Mn-disordered zinc-blende, β' the Mn-ordered zinc-blende, and γ and δ are the NiAs and NaCl structures of MnTe, respectively; (○) heating run (●) cooling run; (▽) from X-ray data.

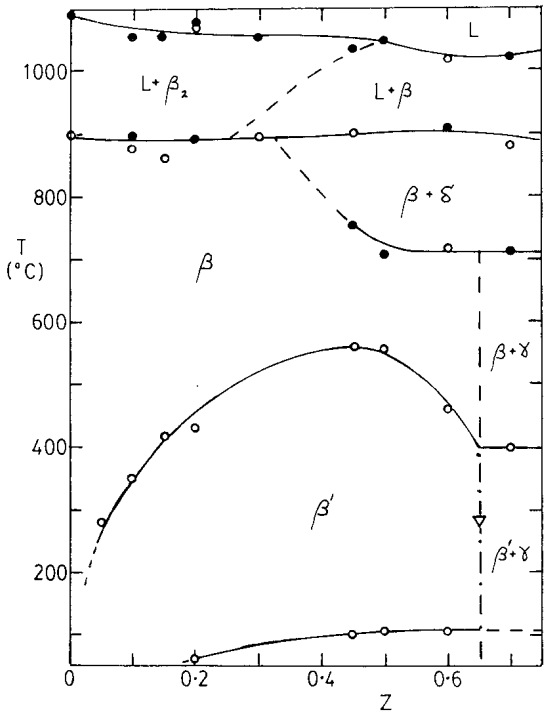

Fig. 5. $T(z)$ diagram for the $x = y$ section: β is the Mn-disordered zinc-blende, β' the Mn-ordered zinc-blende, and γ and δ are the NiAs and NaCl structures of MnTe, respectively; (○) heating run; (●) cooling run; (▽) from X-ray data.

$x = 3y$ sections (figs. 5 and 6), the chalcopyrite phase does not occur, but a wide range of zinc-blende β phase is observed.

With regard to the lower temperature range, i.e. mainly in the range of the single phase solid fields, for the $z = 0$ section (fig. 2), it is seen that the α phase appears at 672 °C for $x = 0$ and that the field achieves a maximum width of approximately $z = 0.28$. For the higher temperature range of this section, the β phase occurs at all compositions, and for $x > 0.28$ it occurs at all temperatures below the solidus curve. In the $x = 0$ section, the lattice parameter data [12] indicate a range of solid solubility in the adamantine phases of $z = 0.59$. For z greater than this, there is two phase behaviour with the γ phase of MnTe with the NiAs structure being observed. As shown in previous work [6], the adamantine single phase fields consist of four different ordered structures, α the

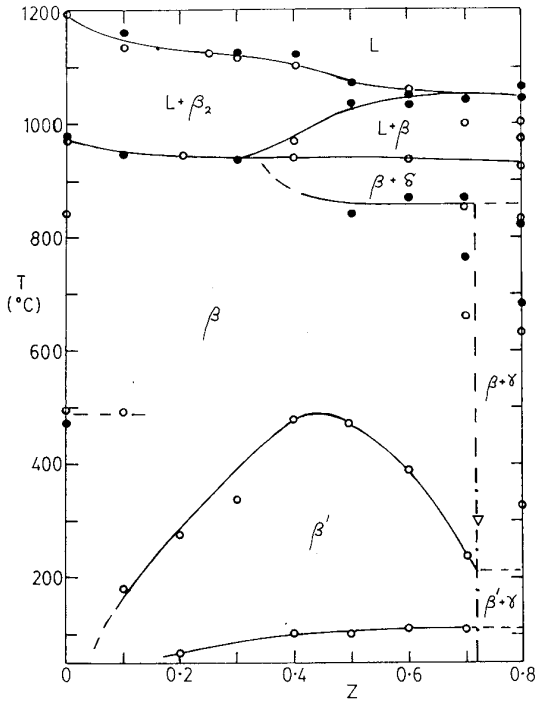

Fig. 6. $T(z)$ diagram for the $x = 3y$ section: β is the Mn-disordered zinc-blende, β' the Mn-ordered zinc-blende, and γ and δ are the NiAs and NaCl structures of MnTe, respectively; (○) heating run; (●) cooling run; (▽) from X-ray data.

Mn-disordered chalcopyrite (dc), α' the Mn-ordered chalcopyrite (oc), β the Mn-disordered zinc-blende (dzb) and β' the Mn-ordered zinc-blende (ozb) forms. However, in the previous $T(z)$ diagram the limit of the oc phase α' was shown as $z = 0.35$, but later measurements of magnetic susceptibility [16] and optical energy gap [17] showed that the α' could be present to the limits of solid solubility in the adamantine phases. Re-examination of the DTA data showed the presence at temperatures in the range 100–200 °C of small peaks corresponding to the α'–β' transition. This modified boundary is shown in fig. 3. In addition, a further transition was observed for $z > 0.2$ at temperatures of the order 100 °C, and the resulting line is also shown in fig. 3. At present, there are no data to indicate the phase conditions below this boundary.

The form of the boundary between the chalcopyrite and zinc-blende phases, being an $(\alpha + \beta)$ two-phase field for $z < 0.20$ and a single line for $z > 0.20$ has been attributed to the ordering of the Mn atoms [6], the change at $z = 0.20$ corresponding to the point where the α–α' boundary meets the $\alpha(\alpha')$–β transition. Very similar results to those described above for the $x = 0$ section have been observed for the $(AgIn)_{1-z}Mn_{2z}Te_2$ diagram [18].

The behaviour of the section $y = 3x$ (fig. 4) in this lower temperature range is similar to that of the $x = 0$ section. Again, α, α', β and β' fields occur and at temperatures below 200 °C, the oc α' phase extends to the limit of solid solubility at $z = 0.60$. Also, at temperatures around 100 °C the boundary corresponding to the unknown transition mentioned above is again observed. In the cases of the $x = y$ and $x = 3y$ sections (figs. 5 and 6), no chalcopyrite phase occurs, but there is a wide range of solid solubility in the zinc-blende structure, to $z = 0.65$ for $x = y$ and to $z = 0.72$ for $x = 3y$. For both of these sections, the boundary corresponding to the unknown transition is observed at approximately 100 °C, as is shown in figs. 4 and 5. Thus this transition is not limited to the chalcopyrite phase, but occurs for the ordered form of both of the adamantine structures.

At the temperatures above the limit of the β field, the diagrams are more complicated and the designation of the phases in the various fields has been guided by the work of Chiang et al. [19] and Aresti et al. [5]. Firstly, two different zinc-blende phases occur [19], accounting for the β_2 phase shown in the various sections here. This β_2 has a composition range not represented by any region of the present investigation but found in the Cu_2Te–In_2Te_3 section. At the higher values of z, two phases fields involving a phase δ occur, and this has been identified [5] as the rocksalt structure shown by MnTe above 1050 °C, but which exists at lower temperatures elsewhere in the general diagram. It is clear that, in general, none of the sections shown are pseudo-binary in character. However, for the $x = 0$ section and for temperatures below 600 °C, pseudo-binary conditions appear to be satisfied to a good approximation.

4. Conclusions

The DTA and X-ray results for the $Zn_{2x}(CuIn)_yMn_{2z}Te_2$ alloys show that a wide range of solid solution occurs for both the chalcopyrite and zinc-blende structures, and that for both structures an ordered form, attributed to the Mn ions ordering on the cation sublattice, occurs below approximately 550 °C for values of $z > 0.05$.

Over the whole composition range, the β phase is bounded by a two-phase ($L + \beta_2$) field. Since the β_2 phase is not represented by any point in the present composition triangle, the diagram cannot be pseudo-ternary nor can any pseudo-binary sections be present.

Acknowledgements

The authors wish to thank Professor L. Garbato and Professor F. Ledda of the Instituto di Fisica dell'Università, Cagliari, Italy, for useful discussions. They are grateful to Mr. G.S. Pérez and Mr. F. Sanchez for technical assistance. Also they wish to thank Consejo de Desarrollo Cientifico Humanistico y Tecnologico (CDCHT), Universidad de Los Andes (ULA) and Consejo Nacional de Investigaciones Cientificas y Tecnologicas (CONICIT) Venezuela for financial support.

References

[1] J.A. Gaj, J. Phys. Soc. Japan 49 (1980) 797.
[2] J.K. Furdyna, J. Appl. Phys. 64 (1988) R29.
[3] M. Quintero, L. Dierker and J.C. Woolley, J. Solid State Chem. 63 (1989) 110.
[4] M. Quintero and J.C. Woolley, Phys. Status Solidi (a) 92 (1985) 449.
[5] A. Aresti, L. Garbato, A. Geddo-Lehmann and P. Manca, in: Proc. 7th Intern. Conf. on Ternary and Multinary Compounds (Materials Research Society, Pittsburgh, PA, 1986) p. 497.
[6] M. Quintero, P. Grima, R. Tovar, G.S. Perez and J.C. Woolley, Phys. Status Solidi (a) 107 (1988) 205.
[7] M. Quintero, R. Tovar, M. Al-Najjar, G. Lamarche and J.C. Woolley, J. Solid State Chem. 75 (1988) 136.
[8] J.C. Woolley, G. Lamarche, A. Manoogian, M. Quintero, L. Dierker, M. Al-Najjar, D. Proulx, C. Neal and R. Goudreault, in: Proc. 7th Intern. Conf. on Ternary and Multinary Compounds (Materials Research Society, Pittsburgh, PA, 1989) p. 479.
[9] M. Quintero, P. Grima, J.E. Avon, G. Lamarche and J.C. Woolley, Phys. Status Solidi (a) 108 (1988) 599.
[10] M. Quintero, P. Grima, R. Tovar, R. Goudreault, D. Bissonnette, G. Lamarche and J.C. Woolley, J. Solid State Chem. 76 (1988) 210.
[11] L. Garbato and F. Ledda, J. Solid State Chem. 30 (1979) 189.
[12] C. Neal, J.C. Woolley, R. Tovar and M. Quintero, J. Phys. D (Appl. Phys.) 22 (1989) 1347.
[13] R. Tovar, M. Quintero, P. Grima and J.C. Woolley, Phys. Status Solidi (a) 111 (1989) 405.
[14] R. Chen and Y. Kirsh, The Analysis of Thermally Stimulated Processes, Intern. Series on the Science of the Solid State, Vol. 15 (Pergamon, Oxford, 1981) p. 97.
[15] L.S. Palatnik and E.I. Rogacheva, Soviet Phys.-Dokl. 12 (1967) 503.
[16] G. Lamarche, J.C. Woolley, R. Tovar, M. Quintero and V. Sagredo, J. Magnetism Magnetic Mater. 80 (1989) 321.
[17] M. Quintero, R. Tovar, M. Dhesi and J.C. Woolley, Phys. Status Solidi (a) 115 (1989) 157.
[18] R. Tovar, M. Quintero, C. Neal and J.C. Woolley, J. Electrochem. Soc., in press.
[19] R.W. Chiang, D.F. O'Kane and D.R. Mason, J. Electrochem. Soc. 113 (1966) 849.